Shear jamming onset in dense granular suspensions

Saisai Cao, Yu Wang, Haoming Pang, Junshuo Zhang, Yuxuan Wu, Shouhu Xuan, and Xinglong Gong

Citation: Journal of Rheology **65**, 419 (2021); doi: 10.1122/8.0000190
View online: https://doi.org/10.1122/8.0000190
View Table of Contents: https://sor.scitation.org/toc/jor/65/3
Published by the The Society of Rheology

Shear jamming onset in dense granular suspensions

Saisai Cao, Yu Wang,[a] Haoming Pang, Junshuo Zhang, Yuxuan Wu, Shouhu Xuan, and Xinglong Gong[b]

CAS Key Laboratory of Mechanical Behavior and Design of Materials, Department of Modern Mechanics, CAS Center for Excellence in Complex System Mechanics, University of Science and Technology of China (USTC), Hefei 230027, People's Republic of China

(Received 15 November 2020; final revision received 13 March 2021; published 7 April 2021)

Abstract

Discontinuous shear thickening and dynamic shear jamming can be observed in the dense granular suspension. Here, we determine the criterion for the occurrence of shear jamming by studying the first normal stress difference N_1 of dense granular suspension in steady-state rheology. When $N_1 = 0$, the suspension is shear jammed, and the frictional contact dominates the framework. The jamming onset stress decreases when the particle volume fraction increases. The lubrication to friction mechanism predicts the occurrence of shear jamming and is consistent with the trend predicted by the Wyart–Cates model. The state of a dense granular suspension can be distinguished in the state diagram via the analysis of N_1. This work can aid understanding of the rheology of concentrated particle suspensions. © *2021 The Society of Rheology.* https://doi.org/10.1122/8.0000190

I. INTRODUCTION

A shear thickening fluid (STF) is a type of granular suspension whose apparent viscosity η rises dramatically when the shear stress τ or shear rate $\dot{\gamma}$ exceeds a certain value [1,2]. Continuous shear thickening (CST), during which η rises mildly, is often observed in suspensions with lower concentrations. Dense granular suspensions can exhibit discontinuous shear thickening (DST) or shear jamming (SJ) behavior when subject to shear [3,4] or impact [5–8]. In particular, when shear thickening occurs in an STF, η rises sharply and the flow curve can even assume an S-shape under stress-controlled rheological conditions [9–12].

The Wyart–Cates (W-C) model [13] can provide a good explanation for the rheological behavior of a dense granular suspension, including during CST and DST. It indicates that the jamming density is a function of the particle pressure in the framework,

$$\phi_J = \phi_m f + \phi_c(1 - f), \tag{1}$$

in which $f(p) \in [0, 1]$ represents the fraction of the frictional contact formed by the ruptured lubrication interaction; ϕ_m and ϕ_c are the maximum frictional and frictionless volume fractions, respectively; and η diverges at ϕ_J. Thus,

$$\eta = \eta_0 \left(1 - \frac{\phi}{\phi_J}\right)^{-2}, \tag{2}$$

where η_0 is the solvent viscosity. According to the W-C theory, the suspension can change from flowable to nonflowable when the shear stress applied to the flowable dense granular suspension exceeds a certain value. SJ is often defined as a nonflowable state. Once the suspension is shear jammed, the applied shear rate decreases to zero. The numerical simulation results are in line with this definition [11,14]. However, in the experiment, this phenomenon is difficult to observe experimentally via conventional rotational rheological tests. The shear rate does not decrease to zero in high-concentration suspensions ($\phi_m < \phi < \phi_c$) that are supposed to be shear jammed within a certain shear stress range [12,15,16]. Faced with this contradictory result, Baumgarten *et al.* [17] explained that the force-chain network is constantly destroyed and reorganized and that this prevents the shear rate from decreasing to 0. Han *et al.* [18] claimed that it is difficult to maintain a uniformly shear jammed state due to the rate fluctuations and boundary slip. Actually, the suspension exhibits elastic properties: once a suspension is shear jammed, a steel ball will not sink in the suspension [19]. Therefore, the classical W-C model is not applicable to the rheological curves of dense granular suspensions or the determination of state transitions in high-concentration suspensions. Other efforts have been focused on the experimental determination of the jamming onset stress of a dense granular suspension under the wide-gap shear geometry. For example, the wide-gap transient flow and the rebound impact of a small ball in the wide-gap Couette geometry were proposed by Peters [19] and Han *et al.* [18,20]. Dhar inferred the jamming stress by fitting the suspension viscosity to various volume fractions and varying the shear stress [21]. Thus far, no criterion has been given directly for the SJ onset in a narrow-gap rheological experiment.

The normal stress differences $N_1 = \sigma_{xx} - \sigma_{yy}$ and $N_2 = \sigma_{yy} - \sigma_{zz}$ are also important rheological parameters [22], where x, y, z are defined as the direction of the shear flow, velocity gradient, and vorticity, respectively. N_1 and N_2

[a]Electronic mail: wyu@ustc.edu.cn
[b]Author to whom correspondence should be addressed; electronic mail: gongxl@ustc.edu.cn

in a Newtonian fluid are equal to 0, while they are complicated in a dense granular suspension with complex rheological behavior. The overall research studies indicate $N_2 < 0$. However, the current N_1 results are very complex [23–25]. N_1 can be either negative or positive depending on the volume fraction and applied stress [26–30]. Negative N_1 is often considered the pure hydrodynamic thickening [31] and observed in a suspension whose particle volume fraction ϕ is relatively low. However, even though the thickening in simulations contains weak frictional contact, N_1 is still negative. A positive N_1 can usually only be observed when a high-concentration suspension is applied with high shear stress. Meanwhile, the normal force [$F = \pi R^2/2(\sigma_{xx} - \sigma_{yy})$ for the cone-plate test system] is greater than 0 in rheology, which means the suspension is trying to push the plate away. This indicates the suspension behaves in elasticity and this behavior is very similar to the shear dilatancy [1]. When the dense granular suspension transitions from hydrodynamic lubrication to frictional contact (L-F) [10,32,33], N_1 changes from negative to positive. Experimentally, positive N_1 indicates that the friction force dominates when it approaches ϕ_m [34]. Moreover, Seto found that the ratio of the first normal stress difference to the shear stress was negative, and tended to 0 when it was more jamming [35]. These existing results inspire us that the jamming onset can be given by the N_1 result. Here, we define the occurrence of SJ as $N_1 \geq 0$. Therefore, the traditional DST area in the experiment is redefined. The experimental SJ in this study corresponds to a portion of the generalized DST state where the dense granular suspension can exhibit elasticity ($N_1 \geq 0$) and flowability ($\dot{\gamma} > 0$). Correspondingly, the DST represents another portion of the generalized DST state where $d\dot{\gamma}/d\tau \leq 0$ and $N_1 < 0$.

The rheological behavior of a dense, polymer-based granular suspension was investigated in this study. Its dynamic SJ flow curves were fitted using a modified W-C model that considered structural hardening and softening. To explore the criterion for SJ, variation of the first normal stress difference N_1 of suspensions with a wide range of particle volume fractions was studied under various shear stresses. The change in the structural orientation angle of each suspension during shear thickening was obtained via an analysis of the N_1 results. Finally, the state transition diagram of a dense granular suspension was summarized in the $\tau - \phi$ plane based on the flow curve and N_1 results.

II. MATERIALS AND METHODS

The dense granular suspension used in this work was a mixture of polystyrene ethyl acrylate (PSt-EA) nanoparticles (diameter 350 nm, density 1.05 g/cm^3) and ethylene glycol. Since the particle and solvent densities were quite similar, sedimentation of the particles was ignored. Rheological tests were performed using a rheometer (Anton Paar MCR302). The test system was equipped with a cone-plate rotor (test diameter 20 mm, cone angle 2°). The test temperature was controlled to 25 °C. To eliminate the initial residual stress in the suspension, preshear was employed before each test.

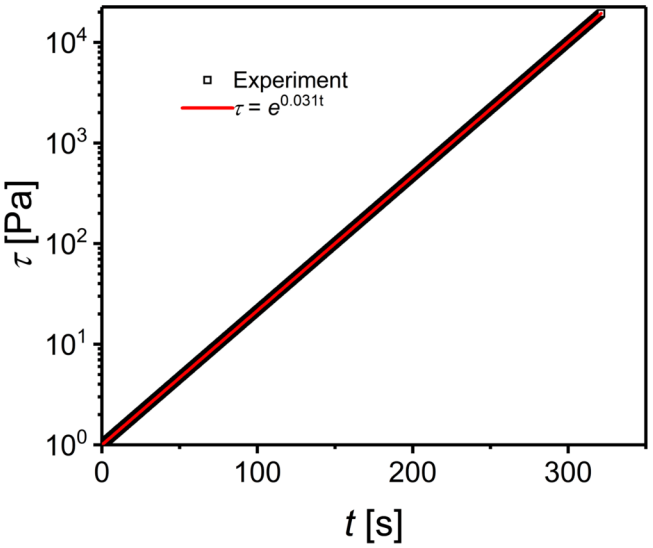

FIG. 1. The applied shear stress τ as a function of time t.

The MCR 302 rheometer had stress- and strain-control modes. In the stress-control mode, the shear stress of the specimen was controlled by controlling the torque on the rotating the rheometer rotor. In this study, the shear stress increased exponentially from 1 to 40 000 Pa in 345 s, and the sampling rate was 4 pts/s. Once the suspension was thrown out of the test area, the test was terminated. The exponential fitting in Fig. 1 reveals that the shear stress growth function was $\tau = e^{0.031t}$. The rate of change of the shear stress remained constant in all experiments.

III. RESULTS AND DISCUSSIONS

A. Rheological flow curve

Figure 2(a) presents the flow curves of suspensions with a wide range of particle volume fractions. The complete results are shown in the supplementary material [36]. When τ is below the threshold for shear thickening $\tau^* = 379$ Pa, η decreases when τ increases, and the suspension exhibits shear thinning. When τ exceeds 379 Pa, η starts to rise and the suspension exhibits clear shear thickening phenomenon. The suspension exhibits the CST characteristics when $\phi = 0.53$ or 0.54, whereas $\dot{\gamma}$ increases monotonically as τ increases. When the volume fraction increases, the suspension exhibits the DST characteristics at $\phi_{DST} < \phi < \phi_m$ (ϕ_{DST} is the critical volume fraction for the occurrence of DST). The flow curve is S-shaped with $d\dot{\gamma}/d\tau \leq 0$. Beyond this region, τ and $\dot{\gamma}$ exhibit positive correlations again. According to the W-C theory, the suspension can be shear jammed as $\phi_m < \phi < \phi_c$ and the jamming onset stress decreases with the particle volume fraction. In our work, the rheological tests indicate that $\phi_m = 0.581$ and $\phi_c = 0.628$. Thus, the suspension is shear jammed when $0.581 < \phi < 0.628$. However, $\dot{\gamma}$ does not decrease to 0 even when τ increases from 1 to 20000 Pa. This indicates that the suspension is shear jammed within a certain shear stress range, but the shear rate does not determine this state transition.

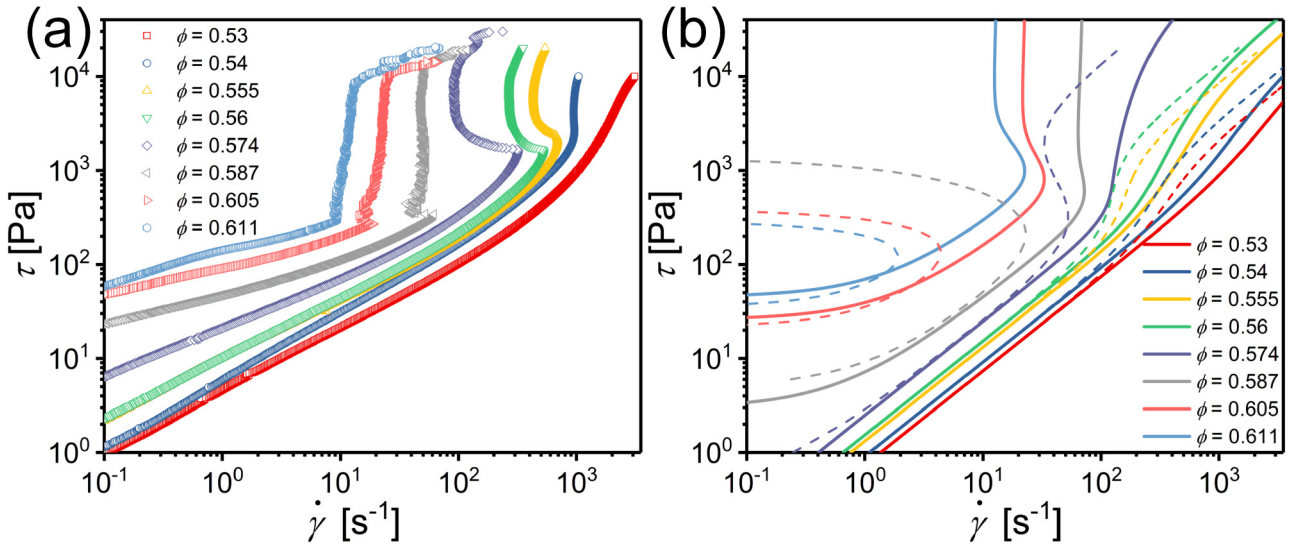

FIG. 2. (a) Flow curves: shear stress τ vs shear rate $\dot{\gamma}$ for suspensions with various concentrations under stress-controlled shear rheology conditions. (b) The flow curves predicted by classical (dashed line) and modified (solid line) W-C models with the volume fraction-dependent yield stress.

According to the classical W-C model, the frictional contact fraction is 1 ($f = 1$) and the shear rate is zero ($\dot{\gamma} = 0$) in the shear jammed state. However, the shear rate remains almost a constant value ($\dot{\gamma} \neq 0$) during the rheological experiment. This implies that $f < 1$. To clarify this conflict, researchers tend to assume that f is a function of time and stress, $f = f(t, \tau)$ [12,16,17]. In this work, we use the equation provided by Baumgarten *et al.* [17],

$$\frac{\dot{f}}{K_0\dot{\gamma}} = H(\hat{f} - f) - Sf, \tag{3}$$

where K_0 is a dimensionless parameter; $\hat{f}$ is the upper bound of hardening; and H and S are the hardening and softening rates, which are functions of the yield stress τ_y [14,37]. In the above equation, $H = (\max(\tau - \tau_y, 0)/\tau^*)^{3/2}$ and $S = 1 + \max(\tau - \tau_y, 0)/\eta_B\dot{\gamma}$ [36]. When f hardens, $f \to \hat{f}$ and the system becomes more jammed. When f softens, $f \to 0$. Hardening and softening of f represent continuous destruction and reorganization of the jamming network under the action of shear. The modified W-C model [Fig. 2(b)] provides a good description of the flow curve: despite the occurrence of SJ, $\dot{\gamma}$ measured by the experiment is not equal to 0 due to continuous destruction and reorganization of the jamming network [38] in the framework. When $\phi_m < \phi < \phi_c$, the suspension can be shear jammed under high shear stress. In this case, the suspension transitions from a fluid state to a solidlike state. The solidlike suspension has the finite strength. When the stress exceeds the failure stress, it is damaged. Therefore, the viscosity of the suspension is finite when SJ occurs because the solid breaks under high stress.

B. Experimental determination of the first normal stress difference

Since $\dot{\gamma} \neq 0$ during SJ, the jamming phase diagram provided by the classical W-C model [36] is not applicable. Moreover, the modified W-C model cannot provide a jamming phase diagram under the criterion that $\dot{\gamma} = 0$. Due to this limitation, we seek a new basis for calculating the occurrence of SJ in dense granular suspension.

We analyze examples where $\phi = 0.56$ and $\phi = 0.594$ in order to consider representative DST and SJ. The complete results are shown in the supplementary material [36]. As shown in Fig. 2, when $\tau \leq \tau^*$, N_1 remains almost constant. However, N_1 exhibits obvious correlation with τ and ϕ when $\tau > \tau^*$. In the CST region [Fig. 2(a)], N_1 is proportional to τ. When ϕ is relatively low ($\phi = 0.53$ and 0.54 in the supplementary material [36]), N_1 can even be positive. To avoid conflicts, we exclude the case of pure CST from the subsequent analysis. During the CST to DST transition, N_1 changes from rising to falling and afterwards becomes increasingly negative such that: $-N_1 \propto \tau$, even the suspension changes from DST to CST again when τ exceeds the upper bound of DST. Once $\phi \geq \phi_m$, SJ occurs. In the DST region, N_1 first exhibits a downward trend in oscillation with τ, in which the oscillation frequency decreases as ϕ increases. Royer *et al.* [34] found that the simulations based on hydrodynamic interactions drive $N_1 < 0$ and predicted that N_1 becomes increasingly negative as the particle concentration increases. Simulations based on friction models with roughened particles could only produce $N_1 > 0$. Their experiment showed that negative contributions to N_1 from lubrication can mask positive frictional contributions at moderate volume fractions. However, at high volume fractions and shear stresses, the friction interactions become dominant and N_1 transitions from negative to positive. The transition of N_1 from falling to rising is caused by increased friction. In addition, N_1 increases with τ due to the influence of increasing frictional contact. The fluctuations in N_1 are similar to the relaxation oscillation of $\dot{\gamma}$ [12]. Fluctuations in $\dot{\gamma}$ are associated with particle migration [16,39]. However, $\dot{\gamma}$ in this work does not exhibit visible oscillation. This reveals that the suspension is anisotropic during DST [27,40]. Frictional contact is often considered to be the origin of DST. Some experimental and numerical results reveal that DST

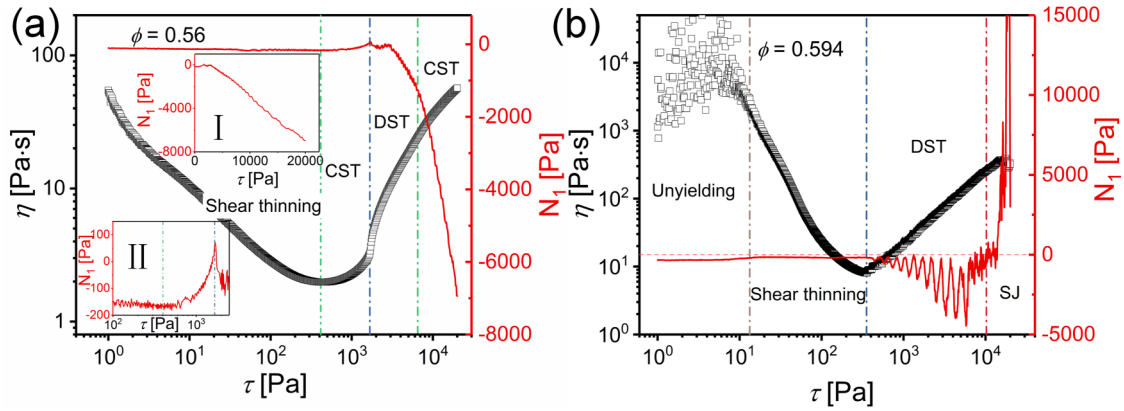

FIG. 3. The apparent viscosity η and first normal stress difference N_1 vs the shear stress τ for (a) $\phi = 0.56$ and (b) $\phi = 0.594$. Inset I: N_1 vs τ in the linear coordinate system indicates that $-N_1 \propto \tau$. Inset II: an enlarged view of N_1 during the CST to DST transition. The positive contribution to N_1 in the CST area originates from the Brownian motion [34].

can be generated when there is only hydrodynamic lubrication between dense, roughened particles [41,42]. According to the literature [10,34], lubrication interactions contribute to making N_1 negative, and the frictional contact can result in $N_1 > 0$. From the numerical simulation of the contact network, one can conclude that there is still a relatively sparse contact effect in the system when the dense suspension exhibits low viscosity [10,25,43]. When $\phi < \phi_m$, the experimental results show that $N_1 < 0$ throughout the shear thickening region. This indicates that the lubrication interaction dominates the system. Although the frictional contact occurs between particles, no continuous force-chain network can be formed due to the low volume fraction of particles. Thus, its influence on N_1 is masked by lubrication. When $\phi_m < \phi < \phi_c$ [Fig. 3(b) and supplementary material [36]], N_1 first decreases and then increases with τ. We note that $N_1 < 0$ in the low shear stress region. However, N_1 becomes positive in the high shear stress region. It can be inferred that hydrodynamic lubrication is dominant within a smaller range of τ. Since the average particle distance is narrower than $\phi < \phi_m$, a local transient contact can form in the direction of the velocity gradient, resulting in oscillation of N_1. Therefore, DST is the result of the combined action of fluid lubrication and frictional contact. After τ exceeds the jamming onset stress τ_J, $N_1 > 0$, the frictional contact is dominant in the system [9,10] and the suspension is shear jammed.

C. The orientation angle

The fluid stress tensor under simple shear is

$$\boldsymbol{\sigma} = \begin{pmatrix} \sigma_{11} & \tau & 0 \\ \tau & \sigma_{22} & 0 \\ 0 & 0 & \sigma_{33} \end{pmatrix}. \tag{4}$$

The corresponding strain rate tensor is

$$\mathbf{D} = \begin{pmatrix} 0 & \frac{\dot{\gamma}}{2} & 0 \\ \frac{\dot{\gamma}}{2} & 0 & 0 \\ 0 & 0 & 0 \end{pmatrix}. \tag{5}$$

In a Newtonian fluid, $\sigma_{11} = \sigma_{22} = \sigma_{33}$. Thus, $N_1 = \sigma_{11} - \sigma_{22} = 0$ and $N_2 = \sigma_{22} - \sigma_{33} = 0$. However, σ_{11}, σ_{22}, and σ_{33} do not equal each other in the dense granular suspension. This may result in a situation where $N_1 \neq 0$ or $N_2 \neq 0$.

The three eigenvalues of the stress tensor $\boldsymbol{\sigma}$ are

$$\lambda_1 = \frac{(\sigma_{11} + \sigma_{22}) + \sqrt{(\sigma_{11} - \sigma_{22})^2 + 4\tau^2}}{2}, \tag{6a}$$

$$\lambda_2 = \frac{(\sigma_{11} + \sigma_{22}) - \sqrt{(\sigma_{11} - \sigma_{22})^2 + 4\tau^2}}{2}, \tag{6b}$$

$$\lambda_3 = \sigma_{33}. \tag{6c}$$

The corresponding eigenvectors are

$$\boldsymbol{n}_1^T = \left(-1, \frac{(\sigma_{11} - \sigma_{22}) - \sqrt{(\sigma_{11} - \sigma_{22})^2 + 4\tau^2}}{2\tau}, 0\right), \tag{7a}$$

$$\boldsymbol{n}_2^T = \left(-1, \frac{(\sigma_{11} - \sigma_{22}) + \sqrt{(\sigma_{11} - \sigma_{22})^2 + 4\tau^2}}{2\tau}, 0\right), \tag{7b}$$

$$\boldsymbol{n}_3^T = (0, 0, 1). \tag{7c}$$

The orientation angle θ is defined as the angle between the direction of compression and the vertical [44]. It is clear that $\cos\theta = (\sigma_{11} - \sigma_{22}) + \sqrt{(\sigma_{11} - \sigma_{22})^2 + 4\tau^2}/2\tau|\boldsymbol{n}_2^T|$ and $\sin\theta = -1/|\boldsymbol{n}_2^T|$. As a result,

$$\tan\theta = \frac{\frac{N_1}{\tau} + \sqrt{4 + (N_1/\tau)^2}}{2}. \tag{8}$$

Finally,

$$\tan 2\theta = \frac{2\tan\theta}{1 - \tan^2\theta} = \frac{2\tau}{N_1}. \tag{9}$$

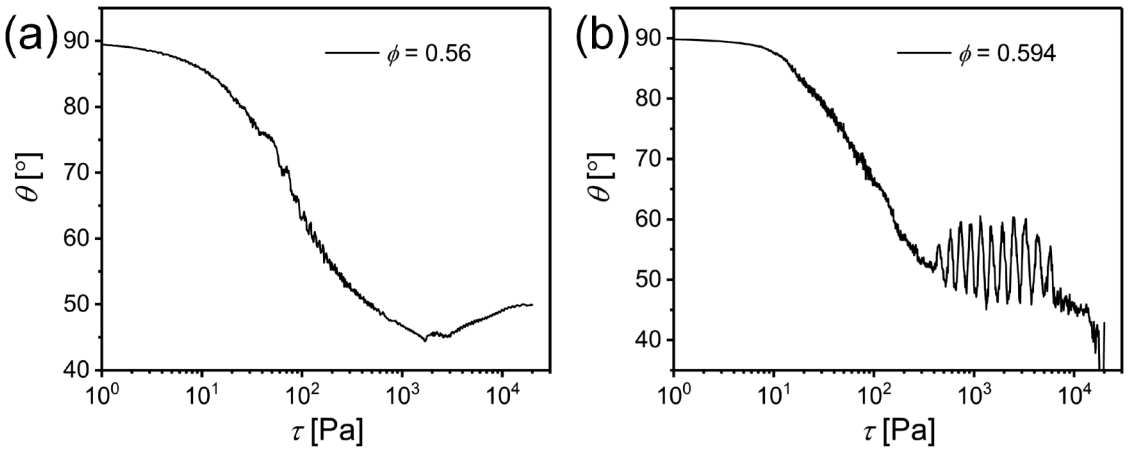

FIG. 4. The evolution of the orientation angle θ vs the shear stress τ when (a) $\phi = 0.56$ and (b) $\phi = 0.594$.

The θ results are calculated based on Eq. (9) and presented in Fig. 4. In general, θ decreases as τ increases. In particular, θ decreases rapidly from nearly 90° in the shear thinning region. $\theta = 90°$ reveals that the direction of the second principal stress inside the suspension in the shear plane is perpendicular to the direction of the shear velocity gradient. This change indicates that the direction of the principal stress axis has been deflected. The difference between the two principal stresses in the shear plane is governed by a linear relationship and τ: $\lambda_1 - \lambda_2/\tau = 2$ in the shear thickened suspension [36]. The orientation angle can explain the N_1 result based on the internal structure. When $\phi = 0.56$, N_1 tends to be more negative as τ increases. However, when $\phi = 0.594$, N_1 transitions from negative to positive as τ increases. From the perspective of N_1, these two results are substantially different. From the point of view of the orientation angle θ, this is because $\theta < 45°$ when $\phi = 0.56$. when $\phi = 0.594$, θ increases from below 45° to above 45°. When $\phi < \phi_m$, θ increases slightly with τ in the DST region. When $\phi \geq \phi_m$, θ decreases in oscillation with τ in DST. When $\theta = 45°$, $N_1 = 0$, and SJ occurs in the suspension.

D. The first normal stress difference as predicted using the lubrication to friction model

Lubrication originates from the squeeze and shear between particles. Frictional contact produces a contact force in the direction of contact and a frictional force perpendicular to the contact direction. As a result, the lubrication interaction and frictional contact affect both σ_{xx} and σ_{yy}. In other words, the hydrodynamic lubrication and frictional contact effect N_1. The decomposition of N_1 can show the influence of the hydrodynamic lubrication and frictional contact in various thickening states visually. In this work, we try to identify the quantitative relationship between lubrication and friction. Singh *et al.* proposed a model that depicts the rate dependent normal stress differences [11]. This model reproduces the contributions of friction and lubrication on the first normal stress difference, in which the lubrication portion diverges at ϕ_c and the friction portion diverges at ϕ_m. It presents the negative to positive transition of N_1. However, the transition zero point is independent of the volume fraction, which is inconsistent with the results obtained in the experiment. In addition, when N_1 is always negative, it has a linear relationship with the shear stress. Although frictional contact occurs in this case, little of it occurs in the framework and its influence is masked by hydrodynamic lubrication. Thus, a negative N_1 can simply be regarded as the result of lubrication. That is, the lubrication portion is linear with respect to the shear stress. The experimental results indicate that N_1 rises sharply after exceeding the transition zero point and tends to infinity. Therefore, we believe that the effect of frictional contact diverges at ϕ_J and propose a friction term that is similar to that of Singh *et al.* in terms of expression. The experimental result indicates that N_1 can be decomposed into two terms: the lubrication term N_{1L} and the friction term N_{1F},

$$N_1 = N_{1L} + N_{1F}. \tag{10}$$

Here, N_{1L} has a linear relationship with τ [24]. According to our experimental results, the first normal stress difference is approximately $N_{1L}^0 = 200$ Pa when the shear stress is 0. This result is derived from the capillary force on the surface of the suspension. The suspension remains stationary when there is no external shear stress. It can be inferred that $\sigma_{xx} = 0$. However, σ_{yy} is not equal to 0. The suspension should be a large droplet on the plate without the upper plate and the side profile is approximately semi-elliptical. Therefore, due to the presence of the upper plate, the suspension is stretched in the vertical direction and $\sigma_{yy} > 0$. It can be inferred that

$$N_{1L} = -0.5\tau - N_{1L}^0. \tag{11}$$

Here, N_{1F} is the contribution from frictional contact. When jamming occurs in a dense granular suspension, N_{1F} diverges at ϕ_J [11],

$$N_{1F} = k\left(1 - \frac{\phi}{\phi_J}\right)^{-2}\tau, \tag{12}$$

in which ϕ_J takes the hardening and softening of f into account [Eq. (3)]. N_{1F} can be determined using the modified

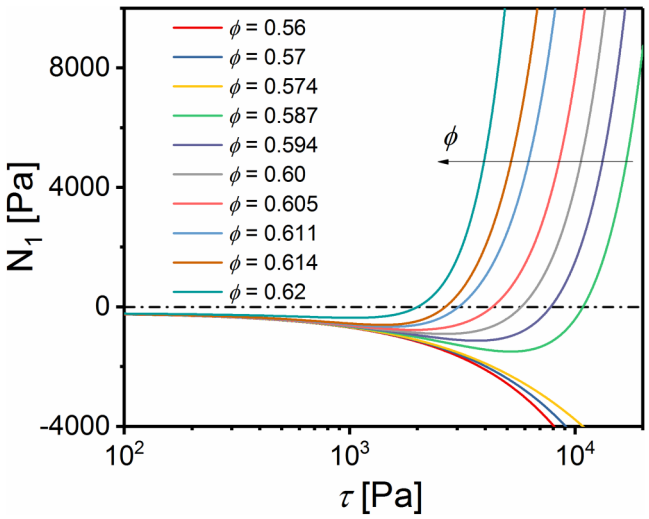

FIG. 5. L-F predictions of N_1 values for suspensions with various volume fractions.

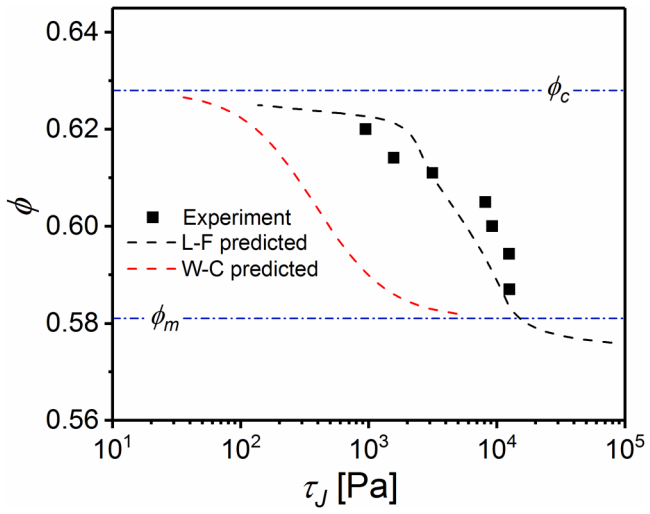

FIG. 7. The volume fraction ϕ as a function of the onset of jamming shear stress τ_J. The black, dashed line shows the result predicted using the L-F theory. The red, dashed line shows the result predicted using the classical W-C model.

W-C model. Figure 5 indicates the overall N_1 comprises lubrication and friction when $k = 0.0025$. It is obvious that the results from the lubrication to friction (L-F) theory correspond well to those from the experiment. When $\phi_{DST} \leq \phi < \phi_m$, N_1 decreases gradually as τ increases. In Fig. 6(a), the value of N_1 depends mainly on N_{1L}. Thus, N_1 decreases linearly as τ increases. When $\phi_m \leq \phi < \phi_c$, N_1 first decreases slowly with τ and then increases. When $N_1 = 0$, the lubrication and friction are balanced and the onset of SJ occurs.

Figures 6(a) and 6(b) depict competition between lubrication and friction. The influence of friction is negligible compared to that of lubrication at $\phi = 0.56$. At $\phi = 0.594$, lubrication is dominant when τ is relatively small. However, as τ increases, the suspension transitions from lubrication to friction, SJ occurs in the suspension, and N_1 changes from negative to positive.

The relationship between the jamming onset stress τ_J and ϕ is analyzed in Fig. 7. It is clear that the suspension can be shear jammed only until $\phi \geq \phi_m$ and that τ_J decreases as ϕ increases. The numerical τ_J predicted using the L-F theory corresponds well to the experiment. This confirms the competition between lubrication and friction mechanisms during the DST-SJ transition. Compared to τ_J obtained via the W-C model, this method identifies a higher threshold for SJ because of the evolution of the internal structure under shear.

As stated in the Introduction, discussion of N_1 has always been of interest to researchers since there are considerable differences between studies. We compare N_1 observed in our experiment to the literature [26,34,41,43,45] in Fig. 8. The values in our work are obtained by averaging data from the 8000–15 000 Pa region. If the test range is lower than this interval, we use a value from a region that is as close as possible to the interval. As shown in Fig. 8, the dimensionless first normal stress difference (N_1/τ) in our work is similar to those found by Royer *et al.*, Mari *et al.*, and Sivadasan *et al.*, who observed a negative to positive N_1 transition as ϕ increased.

E. State diagram

N_1 can be used to distinguish between CST and DST, as well as SJ. Upon combining the flow curve with N_1, the

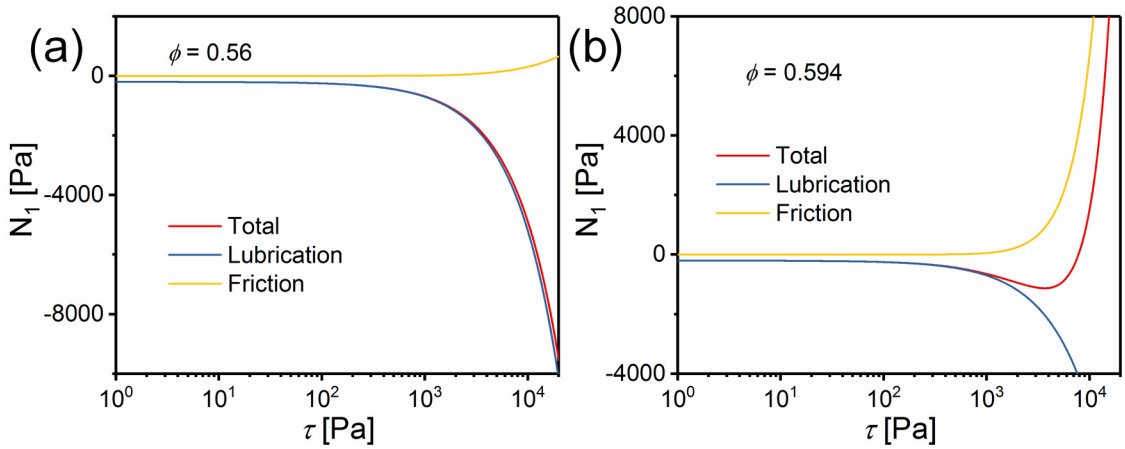

FIG. 6. The contributions of lubrication and friction to N_1 when (a) $\phi = 0.56$ and (b) $\phi = 0.594$.

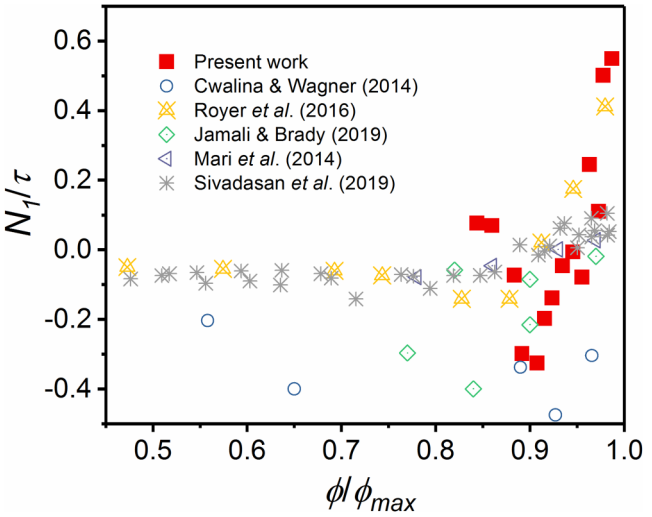

FIG. 8. The dimensionless first normal stress difference (N_1/τ) as a function of ϕ/ϕ_{max}. ϕ_{max} is the maximum packing fraction, which corresponds to ϕ_c in the experiment and ϕ_J^{μ} in the simulation.

suspension can be divided into several distinct states in the $\tau - \phi$ plane (Fig. 9). When $\phi > \phi_0$, the suspension exhibits a significant yield effect. It is not flowable when $\tau < \tau_y$. The yield stress increases with ϕ and diverges at approximately ϕ_c. When the suspension starts to flow, η decreases as τ increases, so shear thinning occurs. The system undergoes shear thickening once $\tau > \tau^*$. When $\phi < \phi_{DST}$, the dense suspension only exhibits CST, $N_1 \propto \tau$. The suspension undergoes CST under lower shear stress when $\phi_{DST} \leq \phi < \phi_m$. When τ reaches the threshold required for DST, $d\dot{\gamma}/d\tau \leq 0$ and N_1 decreases linearly as τ increases. This reveals that the frictional contact is weak in this case

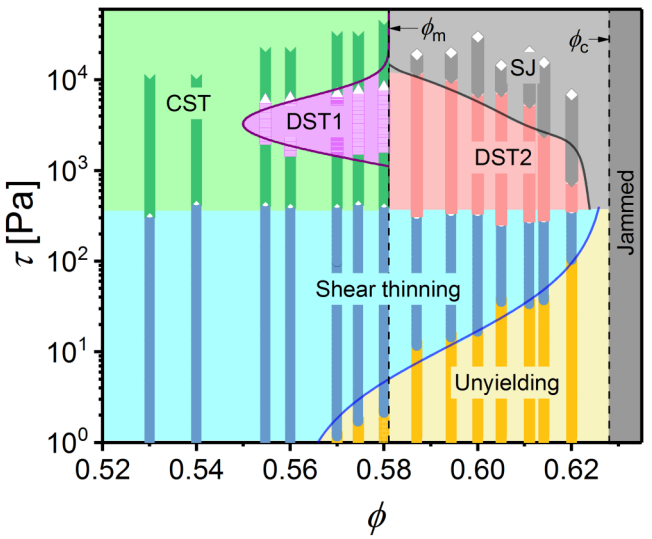

FIG. 9. State diagram for a dense granular suspension with unyielding (yellow), shear thinning (blue), continuous shear thickening (CST, green), discontinuous shear thickening 1 (DST1, purple), discontinuous shear thickening 2 (DST2, pink), shear jamming (SJ, light gray), and fully jammed (gray) regions. The experimental results are shown using darker-colored symbols. The dashed lines indicate ϕ_m and ϕ_c. DST1 and DST2 are separated by ϕ_m. The solid lines show the predicted yield stress (blue), the onset of the SJ stress (black), and the onset of the DST stress (violet).

and hydrodynamic lubrication dominates the suspension [41]. As ϕ increases, the CST area decreases and the CST-DST threshold decreases. When τ exceeds the upper threshold of the DST region, $d\dot{\gamma}/d\tau > 0$. The upper stress threshold of the DST region increases with ϕ. In this case, DST does not cause SJ. The DST in this area is named DST1. It is difficult to observe CST when $\phi_m \leq \phi < \phi_c$. In the DST state, N_1 first decreases and then increases as τ increases. The increasing frictional contact gradually dominates the system. The DST in this case is called DST2. Thus, ϕ_m distinguishes between DST1 and DST2. The suspension transitions from DST to SJ, and this is accompanied by a negative to positive transition of N_1. τ_J decreases with increasing ϕ [21,34]. The suspension is completely jammed when $\phi > \phi_c$. Our state diagram can distinguish the unyielding, shear thinning, CST, DST, and SJ states clearly. The results correspond well to those from previous studies [12,14,18].

IV. CONCLUSIONS

The modified Wyart–Cates model indicated that the force-chain network is constantly destroyed and reconstructed in a shear jammed suspension [17]. In order to determine the SJ phenomenon of suspension via steady-state rheological tests, the basis for judging the occurrence of SJ was explored via N_1. Normally, $N_1 < 0$, and the orientation angle $\theta > 45°$ when $\phi_m \leq \phi < \phi_c$, in the DST region. When N_1 is positive, the frictional contact has surpassed hydrodynamic lubrication and became dominant in the system [34]. This indicates the occurrence of SJ. Our results confirm the competition between lubrication and the friction mechanism during the DST-SJ transition. This work provides help and inspiration for studies of jamming in dense granular suspensions.

ACKNOWLEDGMENTS

Financial support from the National Natural Science Foundation of China (NNSFC, Grant Nos. 11972032, 11772320, 11822209), the fundamental research funds for the Central Universities (No. WK2090050045), and the Strategic Priority Research Program of the Chinese Academy of Sciences (Grant No. XDB22040502) are gratefully acknowledged.

REFERENCES

[1] Barnes, H. A., "Shear-thickening (dilatancy) in suspensions of nonaggregating solid particles dispersed in Newtonian liquids," J. Rheol. **33**, 329–366 (1989).

[2] Brown, E., and H. M. Jaeger, "Shear thickening in concentrated suspensions: Phenomenology, mechanisms and relations to jamming," Rep. Prog. Phys. **77**, 046602 (2014).

[3] Jiang, W., G. Peng, Y. Ma, H. Chen, J. Hu, C. Jia, and T. Zhang, "Measuring the mechanical responses of a jammed discontinuous shear-thickening fluid," Appl. Phys. Lett. **111**, 201906 (2017).

[4] Madraki, Y., G. Ovarlez, and S. Hormozi, "Transition from continuous to discontinuous shear thickening: An excluded-volume effect," Phys. Rev. Lett. **121**, 108001 (2018).

[5] Waitukaitis, S. R., and H. M. Jaeger, "Impact-activated solidification of dense suspensions via dynamic jamming fronts," Nature **487**, 205–209 (2012).
[6] Jerome, J. J., N. Vandenberghe, and Y. Forterre, "Unifying impacts in granular matter from quicksand to cornstarch," Phys. Rev. Lett. **117**, 098003 (2016).
[7] Maharjan, R., S. Mukhopadhyay, B. Allen, T. Storz, and E. Brown, "Constitutive relation for the system-spanning dynamically jammed region in response to impact of cornstarch and water suspensions," Phys. Rev. E **97**, 052602 (2018).
[8] Han, E., L. Zhao, N. Van Ha, S. T. Hsieh, D. B. Szyld, and H. M. Jaeger, "Dynamic jamming of dense suspensions under tilted impact," Phys. Rev. Fluids **4**, 063304 (2019).
[9] Denn, M. M., J. F. Morris, and D. Bonn, "Shear thickening in concentrated suspensions of smooth spheres in Newtonian suspending fluids," Soft Matter **14**, 170–184 (2018).
[10] Morris, J. F., "Lubricated-to-frictional shear thickening scenario in dense suspensions," Phys. Rev. Fluids **3**, 110508 (2018).
[11] Singh, A., R. Mari, M. M. Denn, and J. F. Morris, "A constitutive model for simple shear of dense frictional suspensions," J. Rheol. **62**, 457–468 (2018).
[12] Richards, J. A., J. R. Royer, B. Liebchen, B. M. Guy, and W. C. K. Poon, "Competing timescales lead to oscillations in shear-thickening suspensions," Phys. Rev. Lett. **123**, 038004 (2019).
[13] Wyart, M., and M. E. Cates, "Discontinuous shear thickening without inertia in dense non-Brownian suspensions," Phys. Rev. Lett. **112**, 098302 (2014).
[14] Singh, A., S. Pednekar, J. Chun, M. M. Denn, and J. F. Morris, "From yielding to shear jamming in a cohesive frictional suspension," Phys. Rev. Lett. **122**, 098004 (2019).
[15] Bossis, G., P. Boustingorry, Y. Grasselli, A. Meunier, R. Morini, A. Zubarev, and O. Volkova, "Discontinuous shear thickening in the presence of polymers adsorbed on the surface of calcium carbonate particles," Rheol. Acta **56**, 415–430 (2017).
[16] Hermes, M., B. M. Guy, W. C. K. Poon, G. Poy, M. E. Cates, and M. Wyart, "Unsteady flow and particle migration in dense, non-Brownian suspensions," J. Rheol. **60**, 905–916 (2016).
[17] Baumgarten, A. S., and K. Kamrin, "A general constitutive model for dense, fine-particle suspensions validated in many geometries," Proc. Natl. Acad. Sci. U.S.A. **116**, 20828–20836 (2019).
[18] Han, E., N. M. James, and H. M. Jaeger, "Stress controlled rheology of dense suspensions using transient flows," Phys. Rev. Lett. **123**, 248002 (2019).
[19] Peters, I. R., S. Majumdar, and H. M. Jaeger, "Direct observation of dynamic shear jamming in dense suspensions," Nature **532**, 214–217 (2016).
[20] Han, E., M. Wyart, I. R. Peters, and H. M. Jaeger, "Shear fronts in shear-thickening suspensions," Phys. Rev. Fluids **3**, 073301 (2018).
[21] Dhar, S., S. Chattopadhyay, and S. Majumdar, "Signature of jamming under steady shear in dense particulate suspensions," J. Phys.: Condens. Matter **32**, 124002 (2020).
[22] Pan, Z., H. de Cagny, M. Habibi, and D. Bonn, "Normal stresses in shear thickening granular suspensions," Soft Matter **13**, 3734–3740 (2017).
[23] Guazzelli, É., and O. Pouliquen, "Rheology of dense granular suspensions," J. Fluid Mech. **852**, P1 (2018).
[24] Gamonpilas, C., J. F. Morris, and M. M. Denn, "Shear and normal stress measurements in non-Brownian monodisperse and bidisperse suspensions," J. Rheol. **60**, 289–296 (2016).
[25] Boromand, A., S. Jamali, B. Grove, and J. M. Maia, "A generalized frictional and hydrodynamic model of the dynamics and structure of dense colloidal suspensions," J. Rheol. **62**, 905–918 (2018).
[26] Cwalina, C. D., and N. J. Wagner, "Material properties of the shear-thickened state in concentrated near hard-sphere colloidal dispersions," J. Rheol. **58**, 949–967 (2014).
[27] Jamali, S., A. Boromand, N. Wagner, and J. Maia, "Microstructure and rheology of soft to rigid shear-thickening colloidal suspensions," J. Rheol. **59**, 1377–1395 (2015).
[28] Mari, R., R. Seto, J. F. Morris, and M. M. Denn, "Discontinuous shear thickening in Brownian suspensions by dynamic simulation," Proc. Natl. Acad. Sci. U.S.A. **112**, 15326–15330 (2015).
[29] Cwalina, C. D., and N. J. Wagner, "Rheology of non-Brownian particles suspended in concentrated colloidal dispersions at low particle Reynolds number," J. Rheol. **60**, 47–59 (2016).
[30] Lee, Y.-F., Y. Luo, S. C. Brown, and N. J. Wagner, "Experimental test of a frictional contact model for shear thickening in concentrated colloidal suspensions," J. Rheol. **64**, 267–282 (2020).
[31] Gurnon, A. K., and N. J. Wagner, "Microstructure and rheology relationships for shear thickening colloidal dispersions," J. Fluid Mech. **769**, 242–276 (2015).
[32] Chen, K., Y. Wang, S. Xuan, S. Cao, and X. Gong, "Contribution of frictional contact during steady and oscillatory shear in the discontinuous shear thickening fluid," Smart Mater. Struct. **28**, 045009 (2019).
[33] James. N. M., E. Han, R. A. L. de la Cruz, J. Jureller, and H. M. Jaeger, "Interparticle hydrogen bonding can elicit shear jamming in dense suspensions," Nat. Mater. **17**, 965–970 (2018).
[34] Royer, J. R., D. L. Blair, and S. D. Hudson, "Rheological signature of frictional interactions in shear thickening suspensions," Phys. Rev. Lett. **116**, 188301 (2016).
[35] Seto, R., and G. G. Giusteri, "Normal stress differences in dense suspensions," J. Fluid Mech. **857**, 200–215 (2018).
[36] See supplementary material at https://doi.org/10.1122/8.0000190 for information on material preparation, parameters determination, and formula derivation, as well as detailed experiment data.
[37] Flatt, R. J., and P. Bowen, "Yodel: A yield stress model for suspensions," J. Am. Ceram. Soc. **89**, 1244–1256 (2006).
[38] Behringer, R. P., and B. Chakraborty, "The physics of jamming for granular materials: A review," Rep. Prog. Phys. **82**, 012601 (2019).
[39] Saint-Michel, B., T. Gibaud, and S. Manneville, "Uncovering instabilities in the spatiotemporal dynamics of a shear-thickening cornstarch suspension," Phys. Rev. X **8**, 031006 (2018).
[40] Thomas, J. E., K. Ramola, A. Singh, R. Mari, J. F. Morris, and B. Chakraborty, "Microscopic origin of frictional rheology in dense suspensions: Correlations in force space," Phys. Rev. Lett. **121**, 128002 (2018).
[41] Jamali, S., and J. F. Brady, "Alternative frictional model for discontinuous shear thickening of dense suspensions: Hydrodynamics," Phys. Rev. Lett. **123**, 138002 (2019).
[42] Hsu, C. P., S. N. Ramakrishna, M. Zanini, N. D. Spencer, and L. Isa, "Roughness-dependent tribology effects on discontinuous shear thickening," Proc. Natl. Acad. Sci. U.S.A. **115**, 5117–5122 (2018).
[43] Mari, R., R. Seto, J. F. Morris, and M. M. Denn, "Shear thickening, frictionless and frictional rheologies in non-Brownian suspensions," J. Rheol. **58**, 1693–1724 (2014).
[44] Cates, M. E., J. P. Wittmer, J.-P. Bouchaud, and P. Claudin, "Jamming, force chains, and fragile matter," Phys. Rev. Lett. **81**, 1841–1844 (1998).
[45] Sivadasan, V., E. Lorenz, A. G. Hoekstra, and D. Bonn, "Shear thickening of dense suspensions: The role of friction," Phys. Fluids **31**, 103103 (2019).